Digital Object Identifier (DOI): 10.1109/COMPEL.2014.6877170

Control and Modeling for Power Electronics (COMPEL), 2014 IEEE 15th Workshop on; June 2014

Robustness evaluation of transformerless PV inverter topologies

Holger Jedtberg
Alberto Pigazo
Marco Liserre

Robustness Evaluation of Transformerless PV Inverter Topologies

Holger Jedtberg
Chair of Power Electronics
Christian-Albrecht University of Kiel
Kiel, GERMANY 24143
Email: hje@tf.uni-kiel.de

Alberto Pigazo
Dept. of Computer Systems Engineering and Electronics
University of Cantabria
Santander, SPAIN 39004
Email: pigazoa@unican.es

Marco Liserre
Chair of Power Electronics
Christian-Albrecht University of Kiel
Kiel, GERMANY 24143
Email: ml@tf.uni-kiel.de

***Abstract*—Transformerless PV inverter topologies allow the PV inverter size and weight to be reduced while reaching a higher efficiency. The drawbacks of these topologies are that DC current components at the grid side must be cancelled by means of the employed controller and the number of power devices required to avoid currents through the parasitic capacitor of the PV generator increases.**

These topologies have been analysed in the literature but physical variations of power devices due to the manufacturing process have not been taken into account. This manuscript analyses the effect of such physical variations on the performance of three commonly employed transformerless topologies: H5, HERIC and Half-Bridge NPC. The impact of the parameter variations is compared regarding the efficiencies at different power levels, the European Efficiency and the DC current components. The results indicate that physical variations lead to different behaviors regarding the robustness of the analysed topologies. By means of statistical analyses these differences are obtained and exposed.

I. Introduction

Diverse transformerless topologies for 1ϕ PV inverters have been developed during the last decade. These topologies allow the PV inverter size and weight to be reduced while reaching a higher efficiency. The drawbacks of these topologies are that DC current components at the grid side must be cancelled by means of the employed control technique and the number of power devices required to avoid that the current through the parasitic capacitor of the PV generator increases. Among other manufacturers, SMA, Sunways, Danfoss and Refu have developed their own inverter series based on transformerless topologies (H5, HERIC, NPC and REFU respectively) [1].

The performance of transformerless topologies has been analysed in the literature. A first approach to leakage current in transformerless topologies is given by [2], where these currents are evaluated for a transformerless H4 topology with diverse modulation techniques and LCL filters configurations. H5, HERIC, NPC and FB-ZVR topologies are analysed and evaluated experimentally in [3]. [4] compares the performance of H5, HERIC, H6, FB-ZVR, HB-NPC and Araujo inverter by means of simulation tests in terms of the European Efficiency, output current THD and leakage current. HERIC topology reaches a $\eta_{EU} = 98.27\ \%$ while the the lowest THD corresponds to H6 and no leakage current is obtained in case of NPC topologies. The behaviour of H5, HERIC and H6 topologies is analysed and compared in terms of power losses in [5], where the proposed H6 topology shows a lower efficiency than HERIC but higher than H5 (the measured European Efficiencies in $1\ kW$ prototypes for H5, HERIC and H6 are $96.78\ \%$, $97\ \%$ and $97.09\ \%$) and the minimum leakage current corresponds to H5 ($6\ mA$). Neutral Point Clamped converters are analysed in [6], where it is shown that the European Efficiency reaches $96.4\ \%$, $96.9\ \%$, and $97.2\ \%$ for FB-DCBP, oH5 and PN-NPC topologies respectively. In [7] the losses of a $1\ kW$ prototype are compared by means of simulation tests for H5, oH5, H6, HERIC, HBZVR and HBZVR-D and the leakage currents are measured experimentally. The obtained results show that HERIC topology results in a higher efficiency ($96.05\ \%$) and the lowest leakage current corresponds to HBZVR-D ($42.7\ mA$). Similar analyses have been carried out in [8] and [9] and, in all cases, the obtained results, both in simulation and experimentally, correspond to some power devices selected for simulation purposes or the implementation of prototypes.

This work considers the approach shown in [10], where a statistical approach is proposed for evaluation of the H4 topology and selection of the most suitable power devices for its implementation in 1ϕ PV inverters. This approach would allow the performance of the transformerless topologies for PV inverters to be analysed considering the available technologies for IGBT modules. The analysed topologies are described in Section II. Section III contains the employed statistical method for the analysis by means of simulations and the obtained results. Finally, conclusions are given in Section IV.

II. Studied transformerless topologies for PV inverters

A. H5

The H5 topology consists of a full-bridge with one additional switch in the DC-link as shown in Fig. 1.a which enables the decoupling of the PV inverter from the grid during the freewheeling period of the current [4]. The switches S1 and S3 in the top half of the full-bridge are switched with grid frequency, switches S2, S4, and S5 are operated at high frequency. For creating a positive output voltage S1 is continuously switched on during the positive half wave and S4 and S5 are switched simultaneously. Thus, the current flows through S5, S1, and returns through S4. For obtaining the zero voltage vector S4 and S5 are turned off. During this freewheeling period the current flows through

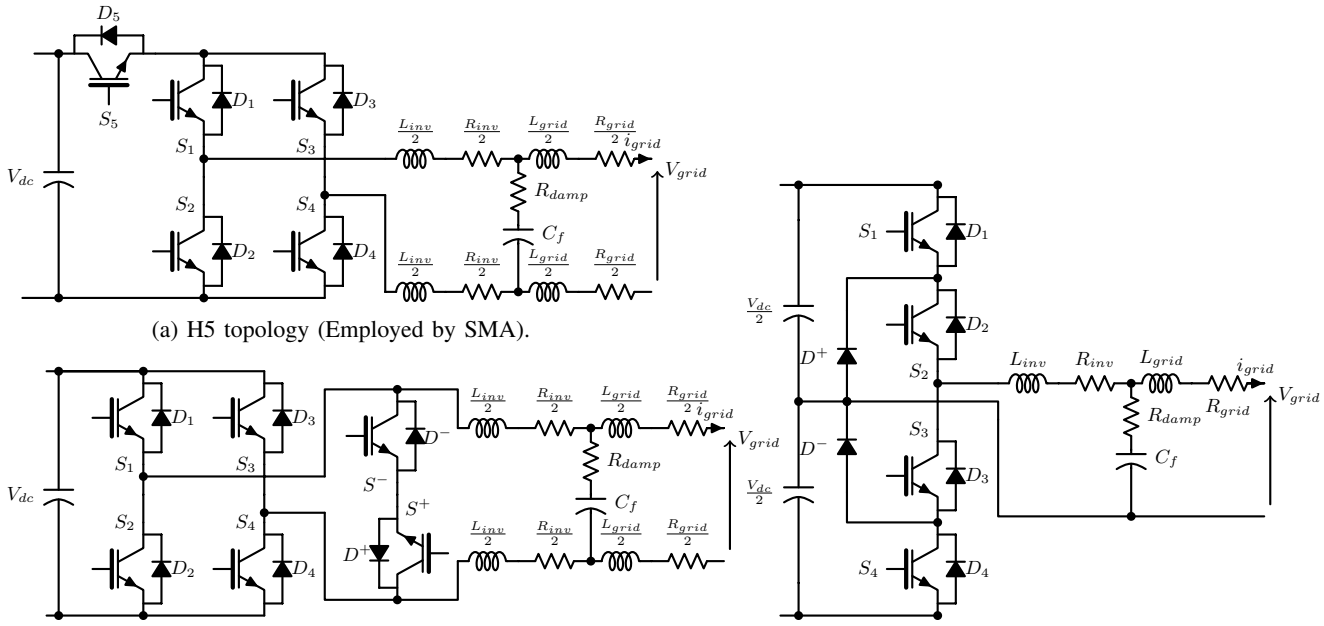

(a) H5 topology (Employed by SMA).

(b) HERIC topology (Employed by Sunways).

(c) HB-NPC topology (Employed by Danfoss).

Fig. 1: Analysed transformerless topologies.

S1 and the anti-parallel diode of S3. The negative voltage output is achieved by the switches S2, S3, and S5. During the negative half wave S3 is continuously switched on with S2 and S5 being switched simultaneously. The current flows through S5, S3, and returns through S2. The zero voltage state is created by switching off S2 and S5, so that the current path leads through S3 and the anti-parallel diode of S1.

The current contains a switching ripple which is equal to the switching frequency resulting in high filtering effort. However, due to the fact that the voltage across the filter is unipolar, low core losses can be expected. Another advantage of the H5 topology can be found in the low leakage current. This is because the voltage to ground V_{PE} is sinusoidal with grid frequency component.

B. HERIC

Based on a full-bridge the HERIC topology (*Highly Efficient and Reliable Inverter Concept*) contains an additional bi-directional switch on the AC side for decoupling the PV inverter from the grid during the freewheeling periods [4]. The topology is shown in Fig. 1.b. As shown, the bidirectional switch is built up of two switches S+ and S- plus their anti-parallel diodes D+ and D-. S+ and S- are switched at grid frequency, S1 to S4 are operated at high frequency. During the positive half wave S+ is turned on and S1 and S4 are switched simultaneously in order to obtain a positive output voltage. The corresponding zero voltage state is achieved by turning off S1 and S4, so that the current flows through S+ and D- on the AC side only. For creating the negative voltage vector S- is continuously turned on during the negative half wave and S2 and S3 are switched concurrently. When S2 and S3 are switched off, the zero voltage state is obtained and the current flows through S- and D+ on the AC side, thus decoupling the PV inverter from the grid during the freewheeling period.

Similar to the H5 topology high filtering effort is also needed for the HERIC topology due to the fact that the current contains a switching ripple equal to the switching frequency. Nevertheless, low core losses are obtained by the unipolar voltage across the filter and a low leakage current is achieved due to a sinusoidal V_{PE}.

C. HB-NPC

In contrast to H5 and HERIC the HB-NPC topology (*Half Bridge - Neutral Point Clamped*) is not based on the full-bridge concept. As can be seen in Fig. 1.c the HB-NPC is a half-brigde consisting of the four switches S1 to S4 and the two clamping diodes D+ and D- which are connected to the neutral grid terminal at the midpoint of the DC-link capacitance [4]. The diodes limit the voltage which is applied to the switches to half of the PV input voltage. This means that the NPC requires twice the PV input voltage in comparison to full-bridge topologies [1].

S2 and S3 are switched with grid frequency, S1 and S4 are operated at high frequency. In order to create a positive output voltage, S1 is switched while S2 is continuously turned on during the positive half wave. With S1 switched off the zero voltage state is created. The current flows through D+ and S2 in the freewheeling period. The negative voltage vector is obtained by switching S4 while S3 is turned on during the negative half wave. The corresponding zero voltage state is created by switching S4 off, which leads the current flow through D- and S3.

In case of the NPC the current also contains a switching ripple which is equal to the switching frequency resulting in

Parameter	Distribution	μ	σ	Mode
IGBT R_{on}	lognormal	-3.9858	0.57921	$13.3\ m\Omega$
IGBT $\frac{L_{on}}{V\cdot I}$	lognormal	-28.6911	0.54508	$0.2574\ nH/kVA$
IGBT $\frac{T_f}{V\cdot I}$	lognormal	-25.7833	0.49124	$4.9848\ ns/kVA$
IGBT $\frac{T_r}{V\cdot I}$	lognormal	-27.0598	0.46334	$1.4284\ ns/kVA$
IGBT $\frac{V_{CE,sat}}{I}$	lognormal	-3.4942	0.46530	$0.0245\ V/A$
Diode R_{on}	lognormal	-4.1475	0.61616	$10.8\ m\Omega$
Diode $\frac{I_f}{V}$	normal	0.075149	0.038791	$75.149\ mA/V$
Diode $\frac{V_f}{I_f}$	lognormal	3.2832	0.65968	$17.254\ V^2/A$
Diode $\frac{dI_f}{dt}$	lognormal	20.9285	0.74512	$-704.71\ A/\mu s$
Diode I_{rrm}	lognormal	3.7343	0.45796	$33.9393\ A$
Diode $\frac{Q_{rr}}{\frac{I_f}{V}}$	lognormal	-9.469	0.75808	$43.459\ \mu F\cdot V/A$
Diode T_{rr}	lognormal	-15.7293	0.52236	$112.29\ ns$

Mode for normal and lognormal distributions are μ and $e^{\mu-\sigma^2}$ respectively.

TABLE I: Parameter distribution of the analysed IGBT modules.

high filtering effort, but here again the core losses are low due to a unipolar voltage across the filter. One remarkable advantage of this topology is that V_{PE} is constantly equal to $-\frac{V_{in}}{2}$ which means that no leakage current is obtained [4].

III. Simulation model

The transfomerless topologies described in the previous section have been analysed by means of simulation tests. These tests allow the evaluation of these topologies subjected to the variations of the electrical characteristics of power devices due to the employed manufacturing processes and the currently available technologies.

A. Controller

In order to compare the obtained results, the same controller, depicted in Fig. 2, has been employed in all cases and only the PWM has been changed according to the switching states described in the previous section. It has been considered that the three analysed topologies are fed by a dc voltage source and the output power can be properly adjusted for each test by changing I_{MPP}, which in practical implementations is provided by the Maximum Power Point (MPP) controller. The reference current $I\sin\omega t$ depends on the available power of the PV system, which will change the amplitude I, and the synchronization signal provided by a Phase Locked Loop (PLL) applied to the grid voltage (v_{grid}). The PLL measures both the amplitude and the frequency of the electrical grid in order to trip the inverter if OUV/OUF condition arises. The reference current for injection purposes is compared to the measured one in order to generate the error signal applied to the current controller, implemented by means of a Proportional-Resonant controller [1].

B. Analysis of the effect of physical variations

In order to compare the performance of each analysed transformerless topology under parameter variations associated to the commercially available power devices, the electrical behaviour of IGBTs and diodes has been modelled by means of 5 and 7 parameters, respectively, whose values change depending on the on employed technology and the manufacturing process.

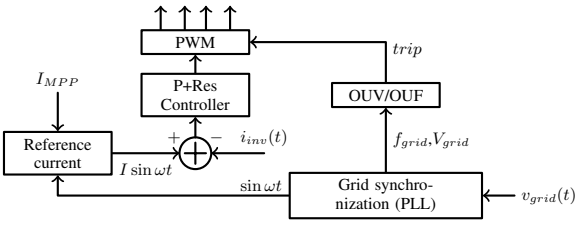

Fig. 2: Employed PV inverter controller.

Each IGBT has been modelled considering the conduction resistance (R_{on}), stray inductance (L_{on}), falling (T_f) and rising (T_r) times and the conduction collector-emitter voltage ($V_{CE,sat}$) [11]. Anti-paralleled diodes in the package have also been modelled considering conduction resistance (R_{on}), forward current (I_f) and voltage (V_f), the rate of change of the forward current ($\frac{\partial I_f}{\partial t}$), the peak recovery current (I_{rrm}), the stored charge (Q_{rr}) and the reverse recovery time T_{rr}. These parameters have been changed during the simulation tests according to the characteristics of the commercially available power devices, which have been statistically analysed in [10]. Table I shows the parameters of the employed probability distribution functions.

IV. Simulation Results

The comparison of the analysed transformerless topologies has been carried out considering the efficiency at each power level (100%, 50%, 30%, 20%, 10% and 5% of the nominal power), the European Efficiency and the DC component of the grid side current.

Monte Carlo (MC) tests have been carried out in order to evaluate the performance of the three analysed transformerless topologies. In order to reduce the number of required points for MC, Latin Hypercube Sampling (LHS) has been applied to the probability distribution functions shown in Table I. The number of simulation points applied at each power level for sampling of the distribution functions is 30. Other required simulation parameters, as depicted in the schematics shown in the previous section, can be found in Table II.

Parameter	Value
L_{inv}	4.7 mH
R_{inv}	0.2 Ω
L_{grid}	2.1 mH
R_{grid}	0.1 Ω
C_f	10 μF
R_{damp}	10 Ω
P_n	3.3 kW
V_{grid}	230 V^{rms}
f_{grid}	50 Hz
f_{sw}	6 kHz
V_{dc}	600 V

TABLE II: Simulation Parameters.

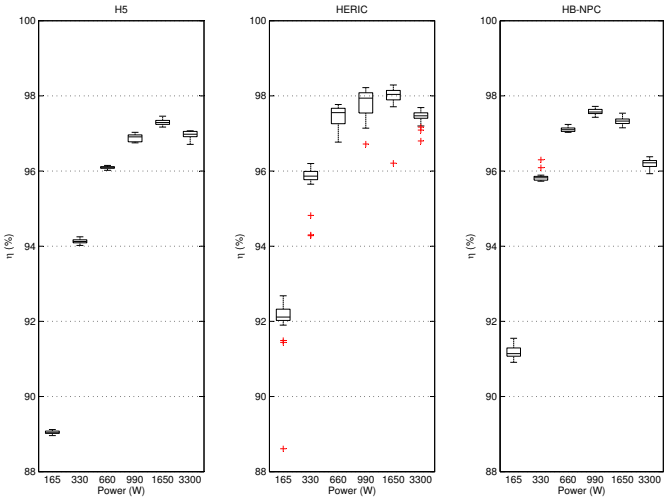

Fig. 3: Distributions of efficiencies per power level.

Fig. 3 shows the obtained efficiencies for H5, HERIC and HB-NPC topologies. As it can be seen, due to the applied simulation points corresponding to the IGBT and diode distribution functions, 6 distribution functions are obtained at each analysed power level. At each power level, the HERIC topology results in the higher efficiency but, as it can be seen, it is also subject to the most parameter variations, which results on the highest variability of the analysed topologies. H5 and HB-NPC show similar variances but different efficiencies. At low power levels, H5 is less efficient than the HB-NPC topology. From this analysis, changes in physical parameters of IGBTs and diodes due to the selected device and its manufacturing process and technology have a low impact on HB-NPC and a high impact on HERIC performances.

The European Efficiency for each analysed topology is shown in Fig. 4 As it can be seen, the highest European Efficiency is reached by the HERIC topology, with a mean $\eta_{EU} = 95.67$ %. NPC and H5 topologies reach 95.5 % and 94.23 % European Efficiencies respectively. These results match the obtained ones in the literature but are a bit lower due to the employed statistical approach. Moreover, relevant info for manufactures is obtained due to the variance. The obtained variances are 2.09 %, 2.63 % and 2.1 % for HERIC, H5 and HB-NPC respectively. As a consequence, H5 shows a higher variability of performance and, hence, it is more sensitive to the

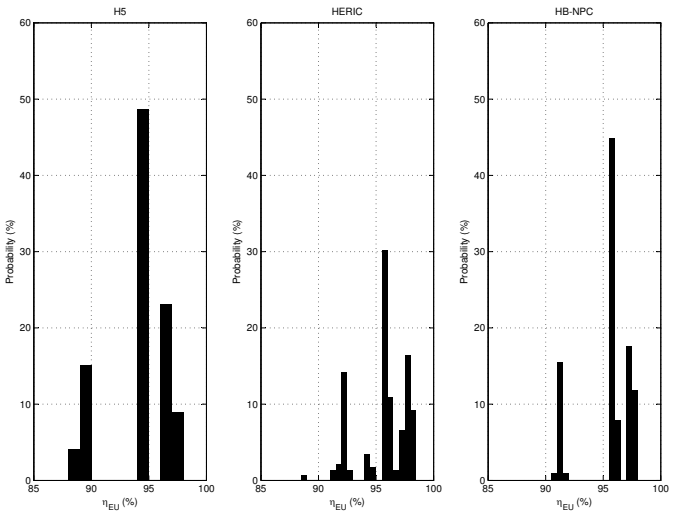

Fig. 4: European Efficiencies.

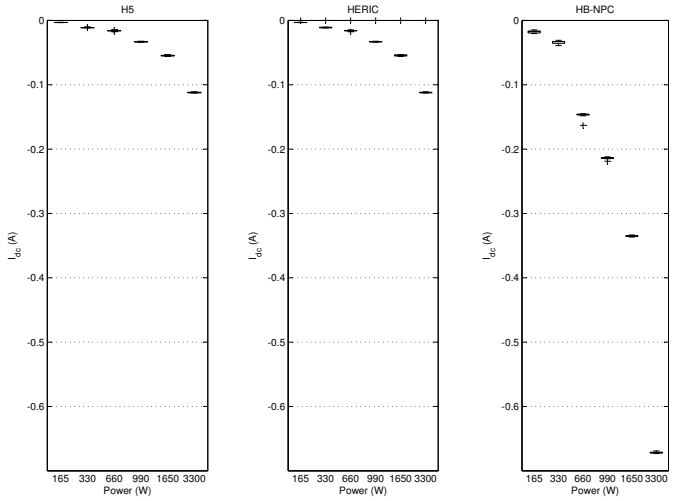

Fig. 5: Measured DC component of the grid side current.

selected power devices. The probability distribution functions in Fig. 4 show that, in worst cases, efficiencies for H5 and HERIC topologies, can fall below 90 % and, in case of HERIC, the distribution of efficiencies is more scattered, reaching a maximum probability of 30.2 % at 95.67 %.

Fig. 5 shows the distribution of the measured DC components of the PV inverter output currents. HB-NPC shows the worst performance, requiring an improved controller in order to avoid such behaviour. The results show that physical variations of IGBTs and diodes have no impact on the DC current component.

V. Conclusion

This manuscript compares the performance of three transformerless PV inverter topologies applying a statistical approach for analysis of the impact of physical parameter variances of IGBTs and diodes. The employed distribution functions correspond to currently available commercial devices, which makes this study relevant for manufactures/investors

trying to select the most appropriate topology considering the available technologies and manufacturing processes. Simulation results showing the efficiencies distribution, the European Efficiency and the injected DC current into the electrical grid are provided. The comparison of the efficiencies per power level shows that parameter variability effects most the HERIC performances and the least the HB-NPC. Thus, it can be seen that the HB-NPC is the most robust topology in terms of parameter variations. The comparison of the variances of the measured European Efficiencies confirms these findings. On top, the fact that the H5 topology shows the greatest variance in terms of European efficiency leads to the conclusion that it is the least robust topology in this context.

REFERENCES

[1] R. Teodorescu, M. Liserre, and P. Rodríguez, *Grid Converters for Photovoltaic and Wind Power Systems*. John Wiley & Sons, 2011, ISBN: 978-0-470-05751-3.

[2] O. López, R. Teodorescu, F. Freijedo, and J. Doval-Gandoy, "Leakage current evaluation of a singlephase transformerless pv inverter connected to the grid," in *Twenty Second Annual IEEE Applied Power Electronics Conference (APEC)*, March 2007, pp. 907–912.

[3] T. Kerekes, "Analysis and modeling of transformerless photovoltaic inverter systems," Ph.D. dissertation, Institute of Energy Technology, Aalborg University, August 2009.

[4] M. C. Poliseno, R. A. Mastromauro, and M. Liserre, "Transformerless photovoltaic (pv) inverters: A critical comparison," in *2012 IEEE Energy Conversion Congress and Exposition (ECCE)*, Sept. 2012, pp. 3438–3445.

[5] L. Zhang, K. Sun, Y. Xing, and M. Xing, "H6 transformerless full-bridge pv grid-tied inverters," *IEEE Trans. Power Electron.*, vol. 29, no. 3, pp. 1229–1238, 2014.

[6] L. Zhang, K. Sun, L. Feng, H. Wu, and Y. Xing, "A family of neutral point clamped full-bridge topologies for transformerless photovoltaic grid-tied inverters," *IEEE Trans. Power Electron.*, vol. 28, no. 2, pp. 730–739, Feb. 2013.

[7] K. F. Tan, N. A. Rahim, H. Ping, and H. Che, "Comparison and analysis of single-phase transformerless grid-connected pv inverters," *IEEE Trans. Power Electron.*, p. 12, accepted for publication.

[8] J. R. Dreher, F. Marangoni, L. Schuch, M. L. da S Martins, and L. D. Flora, "Comparison of h-bridge single-phase transformerless pv string inverters," in *10th IEEE/IAS International Conference on Industry Applications (INDUSCON)*, 2012.

[9] Z. Ozkan and A. M. Hava, "A survey and extension of high efficiency grid connected transformerless solar inverters with focus on leakage current characteristics," in *IEEE Energy Conversion Congress and Exposition (ECCE)*, Sept. 2012, pp. 3453–3460.

[10] A. Pigazo, M. Liserre, F. Blaabjerg, and T. Kerekes, "Robustness analysis of the efficiency in pv inverters," in *IEEE* 39^{th} *Annual Conference of the IEEE Industrial Electronics Society (IECON)*, Nov. 2013, pp. 7015–7020.

[11] *PLECS User Manual: The Simulation Platform for Power Electronic Systems*, Plexim, 2012.

ACKNOWLEDGEMENTS

This study was funded under the ERC Consolidator Grant 2014-2019 in the project "Highly Efficient and Reliable smart Transformer" (HEART).